The Astrophysical Journal, 755:175 (7pp), 2012 August 20 doi:10.1088/0004-637X/755/2/175

DEAD CALM AREAS IN THE VERY QUIET SUN

M. J. Martínez González[1,2], R. Manso Sainz[1,2], A. Asensio Ramos[1,2], and E. Hijano[3]
[1] Instituto de Astrofísica de Canarias, Vía Láctea s/n, E-38205 La Laguna, Tenerife, Spain
[2] Departamento de Astrofísica, Universidad de La Laguna, E-38205 La Laguna, Tenerife, Spain
[3] McGill Physics Department, 3600 rue University, Montréal, QC H3A 2T8, Canada
Received 2012 May 3; accepted 2012 June 20; published 2012 August 7

ABSTRACT

We analyze two regions of the quiet Sun (35.6×35.6 Mm^2) observed at high spatial resolution ($\lesssim$100 km) in polarized light by the IMaX spectropolarimeter on board the SUNRISE balloon. We identify 497 small-scale ($\sim$400 km) magnetic loops, appearing at an effective rate of 0.25 loop h^{-1} arcsec^{-2}; further, we argue that this number and rate are underestimated by $\sim$30%. However, we find that these small dipoles do not appear uniformly on the solar surface: their spatial distribution is rather filamentary and clumpy, creating *dead calm* areas, characterized by a very low magnetic signal and a lack of organized loop-like structures at the detection level of our instruments, which cannot be explained as just statistical fluctuations of a Poisson spatial process. We argue that this is an intrinsic characteristic of the mechanism that generates the magnetic fields in the very quiet Sun. The spatio-temporal coherences and the clumpy structure of the phenomenon suggest a recurrent, intermittent mechanism for the generation of magnetic fields in the quietest areas of the Sun.

Key words: polarization – Sun: dynamo – Sun: surface magnetism

Online-only material: color figures

1. INTRODUCTION

During the last few years, our understanding of the structure, organization, and evolution of magnetic fields in the very quiet Sun (the regions outside active regions and the network) has become increasingly clear. Magnetic fields in the quietest areas of the Sun are relatively weak and organized at small spatial scales, which yields weak polarization signals that are difficult to observe. Until very recently, the general picture of the structure of its magnetism was rather rough: a "turbulent" disorganized field (Stenflo 1982; Solanki 1993; Manso Sainz et al. 2004; Trujillo Bueno et al. 2004). It is now clear that even in very quiet areas, magnetic fields may organize as coherent loops at granular and subgranular scales ($\lesssim$1000 km; Martínez González et al. 2007), that these small loops are dynamic (Martínez González et al. 2007; Centeno et al. 2007; Martínez González & Bellot Rubio 2009; Gömöry et al. 2010), that they pervade the quiet solar surface and may even connect with upper atmospheric layers (Martínez González & Bellot Rubio 2009; Martínez González et al. 2010b).

Yet, this picture is still incomplete. For example, we lack a complete mapping of the full magnetic field vector on extended fields of view because the linear polarization signals are intrinsically weak (they are second order on the transverse magnetic field component), and high spatial resolution maps on linear polarization are rather patchy (Danilovic et al. 2010), which has led to incomplete (and sometimes, physically problematic) characterizations of the topology of the field (Ishikawa et al. 2008; Ishikawa & Tsuneta 2009, 2010).

Here we look for and trace small magnetic loops on extended regions of the quiet Sun observed with the highest spatial resolution. Loop-like structures are a natural configuration of the magnetic field due to its solenoidal character. While they can be traced as individual, coherent entities, they characterize the magnetic field at large, and their statistics and evolution may shed some light on the origin of the very quiet Sun magnetism, in particular, on the operation or lack thereof local dynamo action (Cattaneo 1999). On the other hand, the organization of the field at small scales affects the organization of the magnetic field at larger scales and in higher atmospheric layers (Schrijver & Title 2003; Cranmer 2009) and dynamics (Cranmer & van Ballegooijen 2010).

We find evidence for small-scale loops appearing rather irregularly, as in bursts and clumps. Moreover, wide regions of the very quiet Sun show very low magnetic activity and no apparent sign of organized loops at the detection level of the instruments. These extremely quiet (*dead calm*) regions are an intrinsic characteristic of the statistical distribution of these events.

2. IMaX DATA

This paper is devoted to the analysis of disk-center quiet-Sun observations obtained with the IMaX instrument (Martínez Pillet et al. 2011) on board the SUNRISE balloonborne observatory (Solanki et al. 2010; Barthol et al. 2011). IMaX is a Fabry-Pérot interferometer with polarimetric capabilities at the Fe I line at 5250.2 Å. We analyze two different data sets. Both have the same properties except that they trace different regions of the quiet Sun and were observed at different times, being times series of 22 and 31 minute duration. They consist of five filtergrams taken at $\pm$40, $\pm$80, and +227 mÅ from the Fe I 5250.2 Å line center. The field of view (FOV) is $46.''8 \times 46.''8$ (35.6×35.6 Mm^2), 20 times larger than the one observed by Martínez González & Bellot Rubio (2009). The spatial resolution is about 0.″15–0.″18. The time cadence is 32 s (note that it is 28 s in Martínez González & Bellot Rubio 2009), allowing a noise level of $\sigma = 10^{-3}$ and 7×10^{-4} I_c in the circular and linear polarization, respectively (I_c being the continuum intensity).

3. SMALL DIPOLE COUNTING AND STATISTICS

We look for small magnetic loops in the data set: coherent structures that appear as a dipole in the longitudinal magnetogram (i.e., adjacent positive and negative patches in Stokes

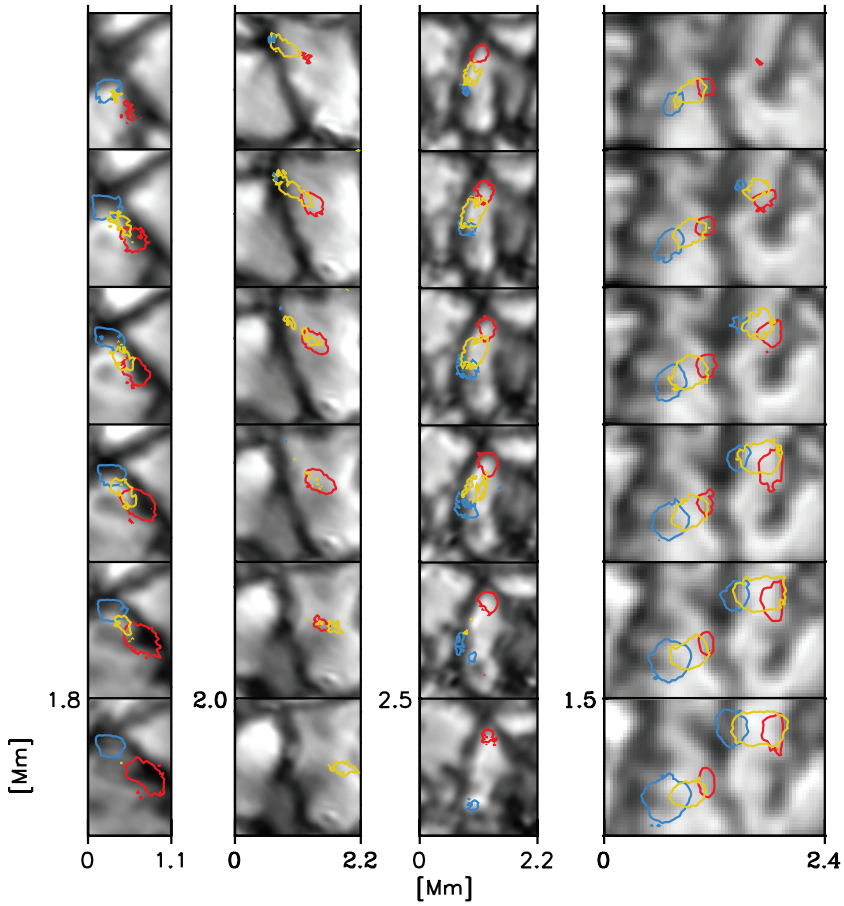

Figure 1. Four examples of small loops found in the IMaX data. The gray-scale background images represent the local granulation. The red and blue contours represent isocontours of magnetic flux density delimiting the positive and negative footpoints of the loop, respectively. The yellow contours represent the linear polarization. The time goes from top to bottom and the time intervals between successive images are not regular. The values of the polarization contours are different but are above the noise level and are chosen in each case to clearly see the loop.

(A color version of this figure is available in the online journal.)

V maps), and a linear polarization patch between them (see Figure 1), which remain identifiable for several (at least two) timeframes (>1 minute).

We looked for small magnetic loops by direct visual inspection. A systematic search was performed in both FOVs at all times for these structures by one of the authors (M.J.M.G.) who recorded the position and evolution at different times of every single event. The method was validated by selecting a small area (10×10 Mm^2) and having a different observer (R.M.S.) independently look for such structures. In this control region, the first observer found $N_M = 37$ loops, and the second one found $N_R = 40$. $N_{M\cap R} = 29$ of them were found by both observers. From those values, the actual number of loops N on the area may be estimated by the Laplace ratio (or Lincoln–Petersen index) for population estimates: $N = N_M N_R / N_{M\cap R} = 51$ (e.g., Cochran 1978); a better, less biased, estimate being $N = (N_M + 1)(N_R+1)/(N_{M\cap R}+1) - 1 = 50$ (Chapman 1951). The variance of this estimate is $\mathrm{Var}(N) \approx (N_M + 1)(N_R + 1)(N_M - N_{M\cap R})(N_R - N_{M\cap R})/[(N_{M\cap R}+1)^2(N_{M\cap R}+2)] = 4.9$ (Chapman 1951).

These formulas have been used in the literature to estimate the size of ecological populations (e.g., Seber 2002; Krebs 2008), and the number of errors in a message (Barrow 1998). The main difficulty for applying the method to our case is that the objects to be counted (the loops as defined in the first paragraph of this section) may not be unambiguous. To guarantee that this condition was fulfilled (i.e., that both observers were identifying and counting the same objects), both observers went over all the structures that the two of them had found in the area a second time, and they had to agree on all the events to be counted as loops.

From this analysis we conclude that the total number of magnetic structures that we find in the whole data set could be underestimated by ∼35%. We note that the clearest those cases (those with the strongest polarization signals, that lasted longer, and were clearly isolated from neighboring magnetic patches) were often found by both observers in the control area. The 35% discrepancy is due to those events found by one observer but not the other; these cases correspond to the subtlest events (those often bordering the detection limit).

We identify 497 small magnetic loops emerging in the observed regions. Taking into account the total time of observation and the spatial area covered, this amounts to an emergence rate of small dipoles of 0.25 loops h^{-1} arcsec^{-2}, increasing to 0.34 loops h^{-1} arcsec^{-2} when we apply the correction for undetected (although present in the data) loops given above. These values are one order of magnitude larger than the previous estimation found by Martínez González & Bellot Rubio (2009), but compatible with Martínez González et al. (2007, 2010b). There are several reasons for the discrepancy. First, the former study covered a relatively small area and, if the emergence is not strictly uniform (as we shall discuss below), the rate can be greatly

underestimated. This fact was already pointed out in Martínez González & Bellot Rubio (2009), where it was noted that there was evidence for preferential emergence regions. The reason why the studies in the near-IR and this paper are in agreement is because, either having a better Zeeman sensitivity (Martínez González et al. (2007, 2010b) used the more sensitive—most importantly to linear polarization—spectral line of Fe I at 1.5 μm) or having a better spatial resolution makes both studies more sensitive, inducing the identification of more (weaker and/or smaller) structures in the field.

Both opposite polarity feet and the linearly polarized bridge between them were tracked during the full loop phase. In most cases (60% of the events), the loop collided with or merged to some degree with a neighboring structure and we could not further trace its individual evolution. This is a common case because at our level of sensitivity and at such spatial resolution, most of the pixels in the FOV show circular polarization, and many show both linear and circular polarization. For the remaining 40% of the cases, the loop's individual history could be traced beyond (and before) the complete loop phase (i.e., when all three polarization patches are seen simultaneously). In nearly half of these cases (56%), both footpoints and linear polarization appear and/or disappear simultaneously because the structure falls below the detection level of the instrument (or it submerges). We called this population of loops "low-lying" (see Martínez González & Bellot Rubio 2009). This population of loops is very particular of the quiet Sun. In 42% of the cases, linear polarization precedes the detection of both footpoints and then disappears before them too. Martínez González & Bellot Rubio (2009) computed the line-of-sight velocity of the loops using the Stokes V zero-crossing shift and verified that all the loops having this same time evolution were rising Ω-loops. We have no reason to think that the loops found in IMaX are a different population. However, we cannot compute the Stokes V velocity in the IMaX data sets analyzed in this paper, hence, there is some doubt about the identification of these loops as rising Ω-loops. In only three instances (2%), we found that first the opposite polarities appear, then the linear polarization between them, then everything disappears, which could be interpreted as the emergence of a U-loop, or, more probably (considering the local evolution of the flow), a submergence of an Ω-loop.

Figure 1 displays four examples of small loops found in the IMaX data. Note that, for the sake of clarity, we have only drawn the contours of interest, avoiding circular and linear polarization patches adjacent to the loop structure. The time runs from top to bottom, the time cadence being irregular. The first and third columns represent typical loops in which the linear polarization disappears at some point in the evolution of the loop while the footpoints stay in the photosphere (probably rising Ω-loops). However, these two loops have some peculiarities that differentiate them. The loop in the first column appears at the border of an expanding granule. As the granule expands, the entire loop is dragged by the plasma flow. The loop in the third column contains a linear polarization signal with a gap in between. These two peculiarities are a consequence of the spatial resolution of the IMaX data that allows us to trace the dynamics of the linear polarization.

The loop in the second column of Figure 1 has another linear polarization patch with curious dynamics. It seems that, somehow, the negative footpoint is disconnected from the positive one (i.e., the loop breaks) and that it connects somewhere else to the right of the positive footpoint. Of course, this is just a visual impression. The example in the fourth column is an example of two loops appearing very close in time and in space. They also disappear more or less at the same time, hence, one could think this is evidence of a sea serpent magnetic field line. Note also that the rightmost loop rotates.

All the observed dipoles are smaller than ∼1 Mm (center-to-center distance between the two opposite polarity patches), becoming increasingly more abundant at smaller scales, with most of the observed dipolar structures being ∼0.4 Mm (Figure 2(a)). This is barely three times the spatial resolution limit of IMaX, which suggests that the detection and our statistics might be limited by the instrument. The tilt angle of these dipoles is uniformly distributed, meaning that it does not follow Hale's polarity law. This last result is consistent with Martínez González & Bellot Rubio (2009) and even with the behavior of the smallest ephemeral regions. Figure 2(b) displays the distance between footpoints with respect to the separation between them at the initial time. Therefore, positive values mean that the footpoints separate with time and negative ones indicate that the footpoints approach each other. On average, the distance grows linearly with time with a velocity of $V_d = 0.9$ km s^{-1}, comparable to typical granular values. This indicates that the loops passively follow the granular flows, as expected from weak magnetic features (Manso Sainz et al. 2010).

The magnetic properties of these small dipoles are represented in Figures 2(c) and (d). They are obtained by inverting the data in the weak field approximation following Martínez González et al. (2012). The magnetic flux has been computed in the area containing the observed signal. The frontier has been defined by eye (as an isocontour of magnetic flux density) and hence is slightly different for the different structures. The magnetic flux density is the mean value of the magnetic flux densities in this same region. The magnetic flux of the loops can be explained with a power law using the exponent found by Parnell et al. (2009). This means that the population of small dipoles follows the population of magnetic fields in the quiet Sun. But looking at the histogram of magnetic flux densities, the loops are located at the tail end of the histogram; it is mostly in the range 10–20 Mx cm^{-1}, i.e., 10–20 G if the magnetic field were uniformly distributed and volume-filling. This is compatible with the results of Martínez González et al. (2010a) who state that, in the quiet Sun, the larger the signal the larger the degree of organization of magnetic fields.

4. SPATIAL DISTRIBUTION

Although small-scale loops are found all over the observed areas, their spatial distribution does not seem to be completely uniform (Figure 3). It can be observed that, at some locations, loops appear repeatedly and successively as in bursts, forming clusters, a behavior that has been noticed before by Martínez González & Bellot Rubio (2009), who pointed out that, often, the appearance of loops made it more likely that new ones were later detected nearby. On the other hand, extended areas seem to be noticeably empty of such events, as if voids appeared in the distribution. However, this may be deceiving since voids are also formed even in strictly uniform distributions of points (Betancort-Rijo 1990, 1991).

A quantitative analysis was performed to determine if these voids are statistically significant. This requires in the first place, an unambiguous definition of "void," a nontrivial task in itself (see, e.g., Kauffmann & Fairall 1991, Tikhonov & Karachentsev 2006, and discussions therein). We adopted the simplest definition here and considered only voids of circular

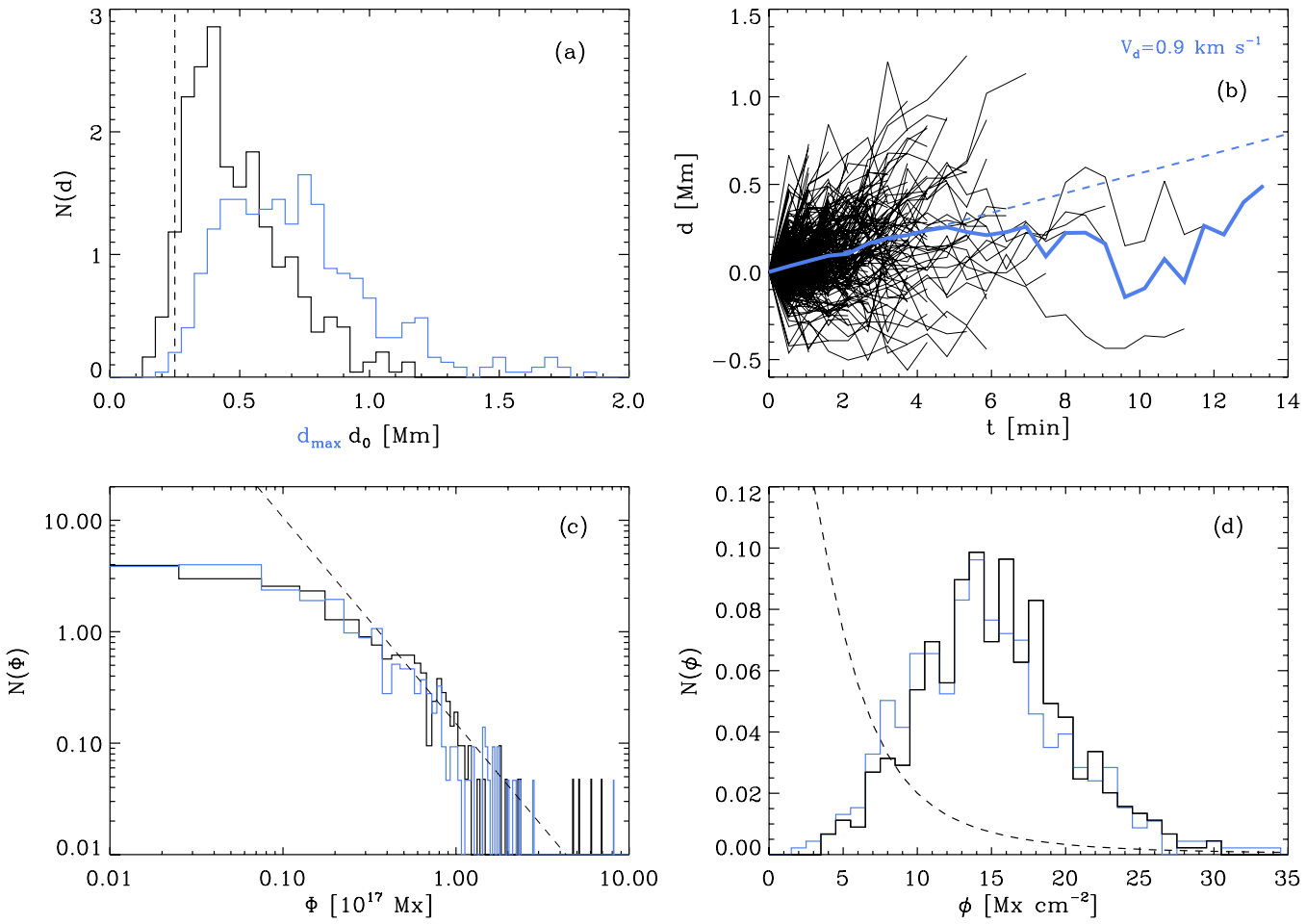

Figure 2. Panel (a) displays the distribution of the initial distance between footpoints (black line) and its maximum extent (blue line). The vertical dashed line represents the mean diameter of the footpoints at the initial time of detection (when the two footpoints are visible for the first time). Panel (b) displays the time evolution of the footpoints' distance with respect to the initial footpoint separation. The thick blue line represents the average and the dashed line is the linear fit. From the slope of this fit we infer the velocity of the footpoint separation of the small dipoles. Panels (c) and (d) represent the histograms of the magnetic flux and the magnetic flux density of the footpoints of the loops, respectively. The black lines represent the positive values while the blue lines are the negative ones. The dashed line corresponds to a power law using the exponent found by Parnell et al. (2009). Note that the proportionality coefficient is different since the fluxes have been obtained with two different instruments and probably have an offset.

(A color version of this figure is available in the online journal.)

shape: the largest empty circle that can be fit in a given region of the point field—equivalently, an empty circle limited by three points of the distribution.[4]

If the loops appeared uniformly on the solar surface, then the probability of finding a void of area between A and $A + dA$ within the FOV (square surface of area L^2) would be (see the Appendix)

$$P(A)dA = \frac{2}{N_{\rm voids}}(L-r)^2\frac{(nA)^2}{A}e^{-nA}ndA, \qquad (1)$$

where $A = \pi r^2$, n is the surface density of points, and $N_{\rm voids}$ is the total number of voids expected in the FOV, which is given by Equation (A1). For the two data sets studied here $L = 31$ Mm (which is slightly smaller than the nominal FOV because we have excluded the apodized exterior area), and $n = 0.22$ Mm^{-2}. Note that we only need a single value of n since the number of loops detected in both data sets is very similar (i.e., 248 and 249 events).

Figure 4 shows the number of voids per unit area in both data sets and for the corresponding Poisson distribution. Except for the smallest areas, the distribution of large circular voids in the first data set is not significantly different from the uniform one. On the second data set, however, apart from the overabundance of small-scale voids, large circular voids seem to be significantly more abundant than a strictly uniform distribution would suggest. Actually, for the parameters found for these observations, the probability of finding a circle with an area larger than $A = 35$ Mm^2 (equivalently, a diameter larger than 3.3 Mm) is very low (3×10^{-4}; see the inset plot in Figure 4). We conclude, therefore, that there is statistical evidence for the two voids marked in Figure 3(a) to be real and not due to chance. Moreover, the overabundance of small voids is interpreted in terms of a clumpy structuring (see how loops appear in clumps, like a gurgle phenomenon, in Figure 3).

In order to relate the distribution of loops (and the voids) to the global magnetism in the observed area, Figure 3 shows the integrated longitudinal (in black and white) and transverse

[4] This is certainly an overabundant definition: several overlapping circles may be found covering what we intuitively consider a single "void." Algorithms might be devised to merge circles and to find a definition closer the intuitive meaning (Gaite 2005; Colberg et al. 2008). This "overcounting" is, however, of no importance for our calculating the probability of finding a void larger than a given size (roughly, all voids are overcounted equally), and we will use this much simpler approach which avoids numerical technicalities.

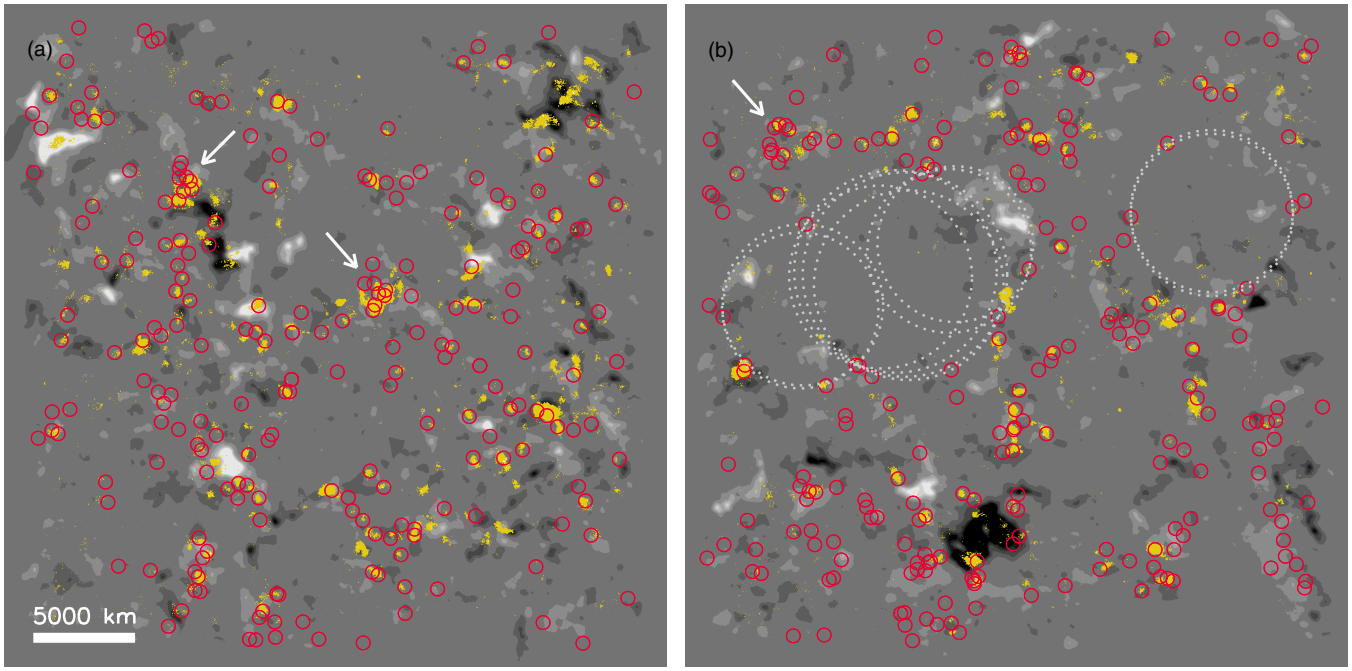

Figure 3. Magnetograms of the two areas analyzed in this paper integrated for the whole observational period. The gray scale has been saturated to show just the most strongly magnetized regions (otherwise, virtually all pixels in the FOV show a detectable signal above noise level). Yellow patches show the average linear polarization signals after correcting for the bias according to Martínez González et al. (2012), and therefore, they are patches with a reliable detection of the transversal component of the magnetic field. Red circles show the average position (between both footpoints) of the 219 (panel (a)) and 216 (panel (b)) small-scale loops detected in both data sets. The trajectories they follow while they evolve are comparable to the size of the circles. The two large areas covered by the dotted circles in panel (b) mark the two *dead calm* regions with a statistically significant lack of (detectable) magnetic loops. Note that they show low magnetic activity too. Arrows indicate a few *hotspots* where several loops appear and disappear at approximately the same position successively over an extended period of time.

(A color version of this figure is available in the online journal.)

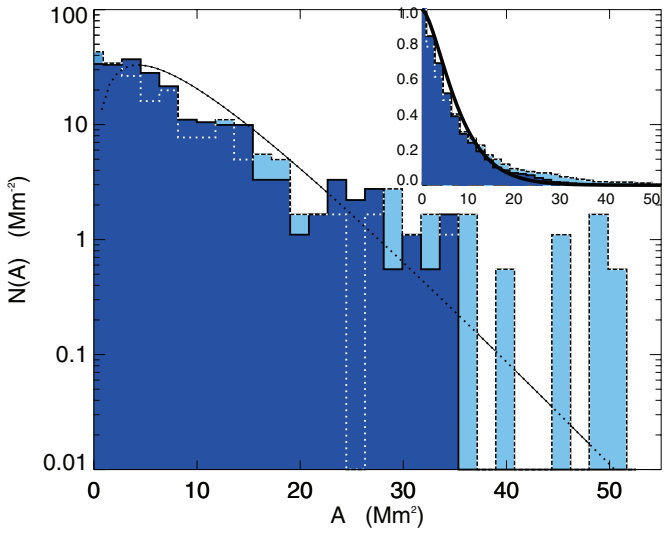

Figure 4. Number of voids per unit area in the two data sets. Dark blue and cyan histograms correspond to the data shown in Figures 3(a) and (b), respectively. Solid line shows $N(A)$ for a Poisson distribution of points with $n = 0.22\ \mathrm{Mm}^{-2}$ (we use a single value since we observe almost the same number of loops in both data sets, i.e., 248 and 249 loops). The inset window represents the probability of finding an area $\geqslant A$. The x-axis is the area A in Mm^2.

(A color version of this figure is available in the online journal.)

(in yellow) magnetograms for the two observations. When dealing with the linear polarization, one has to remember that it is a biased estimator of the transversal field component. In the plot, this bias is statistically partially removed as follows: we compute the bias for a percentile 95 when the observations are pure noise (see Martínez González et al. 2012; note that this bias value depends on each pixel, i.e., on the actual intensity profile). This means that the "real" transverse magnetic will be below this bias value with a probability of 95%. We have decided to set all the values smaller than this bias at 0. Figure 3 shows only the statistically significant patches of linear polarization appearing at all the observed times. The positions of the loops do not seem to be clearly correlated with the longitudinal magnetogram, but the voids encircled by the loops show less magnetic activity than other areas in the FOV. Considering the correlation with linear polarization, this suggests that most of the linear polarization signals that are detected are associated with loop structures embedded in the formation region.

5. DISCUSSION

It is known that even in very quiet areas of the Sun magnetic fields may organize naturally forming loops at granular scales. In this study we extended this observation to the smallest spatial scales observable (100–1000 km), finding an increasing number of loops at smaller scales up to the resolution limit. This finding suggests that the organization of magnetic fields might continue beyond that limit. We cannot reconstruct the complete magnetic field topology because (1) the finite spatial resolution of our observations is (perhaps inherently) above the organization scale of the magnetic fields, and (2) we lack linear polarimetric sensitivity, which gives us only fragmentary information on the transversal (horizontal) component of the magnetic fields. Due to these limitations the loop structures that we observe are biased toward those that are relatively large and relatively strong with respect to the magnetic flux density in the neighboring areas. We found evidence that the loops thus detected are not randomly distributed on the solar surface, but rather that they may appear in bursts, and that they are noticeably absent from extended areas which are, also, only weakly magnetized.

It is not yet clear what the nature of the magnetic fields in the quiet Sun is—what are the fundamental physical mechanisms involved in their generation and evolution? The presence of these *dead calm* areas in the quiet Sun (and small-scale loop hotspots) represents an important constraint on the origin of magnetic fields in the very quiet Sun and on the dominant dynamic and magnetic mechanisms taking place there.

It is thought that the magnetism of the quiet Sun can be the result of the emergence of underlying organized magnetic fields (Moreno-Insertis 2012) or the dragging of the overlying canopy fields (Pietarila et al. 2011). It would then be necessary to understand why there are emergence hotspots and dead calm areas. Another possibility is that they are just a recycling of the decay of active regions as they diffuse and migrate to the poles. But it seems unlikely that such random walking would lead to the kind of organized structures and spatial patterns reported here. It is also possible that they are linked to some type of dynamo action taking place on the solar surface (Cattaneo 1999). It now seems clear that coherent velocity patterns are a requisite for dynamo action to take place (Tobias & Cattaneo 2008). The most obvious coherent velocity pattern in the solar surface is granulation. If this velocity pattern is involved in some dynamo action, it is reasonable that it forms coherent magnetic structures (such as the loops), although these do not need to be organized at the same granular scales; it could well be that they form intermittent patterns like the ones observed here. Actually, theoretical considerations (Chertkov et al. 1999) and laboratory experiments (Ravelet et al. 2008) support the idea that the onset of turbulent dynamo action may be highly intermittent and bursty. Finally, it could just be that these small-scale loops represent the far tail of a continuous range of structures from a global dynamo, just lying at the other end from sunspots. Their spatial statistics would then reflect the velocity patterns on the last (shallowest) layers of magnetic field emergence.

Future models that we construct to understand the generation of magnetic fields in the very quiet Sun have to explain the spatio-temporal coherences that we report. Further work is needed to extend these results in larger areas of the Sun and along the solar cycle.

We especially thank Dr. Juan Betancort Rijo for very helpful discussions on the determination of the statistics of voids, which have improved the paper and strengthened the conclusions. The contribution of Eliot Hijano to this work was in the frame of the summer grants offered by the Instituto de Astrofísica de Canarias. We also thank Valentín Martínez Pillet for helpful discussions. Financial support by the Spanish Ministry of Economy and Competitiveness through projects AYA2010-18029 (Solar Magnetism and Astrophysical Spectropolarimetry) and Consolider-Ingenio 2010 CSD2009-00038 is gratefully acknowledged.

APPENDIX

DERIVATION OF EQUATION (1)

We derive Equation (1) adapting to our case some arguments of the strategy by Gaite (2009). The probability that three points $i = 1, 2, 3$ distributed at random (uniformly) on a square with area $A_t = L^2$, have coordinates between x_i and $x_i + dx_i$, y_i and $y_i + dy_i$ ($0 \leqslant x_i \leqslant L$ and $0 \leqslant y_i \leqslant L$), is $(1/A_t^3) d^3x_i d^3y_i$. With the change of variables $x_i = x_c + r\cos\theta_i$, $y_i = y_c + r\sin\theta_i$, we may express the probability for the center of circumcircle of the three points to lie between x_c and $x_c + dx_c$, y_c and $y_c + dy_c$, its radius between r and $r + dr$, and the azimuthal angles of each point between θ_i and $\theta_i + d\theta_i$, then, as $dx_c dy_c dr d^3\theta_i |J(r, \theta_i)|/A_t^3$, where $J(r, \theta_i) = r^3(\cos\theta_1(\sin\theta_2 - \sin\theta_3) + \cos\theta_2(\sin\theta_3 - \sin\theta_1) + \cos\theta_3(\sin\theta_1 - \sin\theta_2))$ is the determinant of the Jacobian matrix.

The probability of such a circle to lie between the bounds of the large square and its radius to be between r and $r + dr$ is $P_{\rm in}(r)dr = 24\pi(L - r)^2 r^3 dr/A_t^3$, where x_c and y_c have been integrated between r and $L - r$, and θ_i between 0 and 2π, taking into account that the integral of the angular part of $|J(r, \theta_i)|$ is $24\pi^2$. Alternatively, the probability density of the area $A = \pi r^2$ of such a circle is $P_{\rm in}(A)dA = 12(L - r)^2 A dA/A_t^3$.

On the other hand, in a homogeneous Poisson field with density $n = N_t/A_t$ (N_t points randomly distributed over an area A_t), the probability of finding k points in a region of area A is $P_k(A) = (nA)^k/k!\mathrm{e}^{-nA}$. Therefore, the probability of the circumcircle of three points to be void is $12(L - r)^2 A P_o(A) dA/A_t^3$.

Finally, N_t points determine $N_t(N_t - 1)(N_t - 2)/3! \approx N_t^3/3!$ ($N_t \gg 1$) different triplets (hence, possible circles), and the number of void circles with areas between A and $A + dA$ within the square bounds is $2(L - r)^2 A\mathrm{e}^{-nA} n^3 dA$.

The total number of void circles is

$$\begin{aligned} N_{\rm voids} &= \int_0^{N_m} 2(L - r)^2 N\mathrm{e}^{-N} n dN \\ &= \frac{2}{\pi}\left[2(1 + 2N_m) - \mathrm{e}^{-N_m}\left(2 + N_m^2\right)\right. \\ &\quad \left. - 3\sqrt{N_m\pi}\,\mathrm{erf}[\sqrt{N_m}]\right], \end{aligned} \tag{A1}$$

where $N_m = n\pi L^2/4$ and $\mathrm{erf}(x)$ is the error function (Abramowitz & Stegun 1972). The probability of voids of area A with our constraints is then the number of voids of area A divided by the total number:

$$P(A)dA = \frac{2}{N_{\rm voids}}(L - r)^2 \frac{(nA)^2}{A}\mathrm{e}^{-nA} n dA. \tag{A2}$$

For a large total area A_t ($L, A_t, N_m \to \infty$ at constant n), then $P(A)dA = ((nA)^2/A)\mathrm{e}^{-nA} dA$, which coincides with the analysis of Politzer & Preskill (1986).

REFERENCES

Abramowitz, M., & Stegun, I. A. 1972, Handbook of Mathematical Functions (New York: Dover)
Barrow, J. D. 1998, in Impossibility (Oxford: Oxford Univ. Press), 83
Barthol, P., Gandorfer, A., Solanki, S. K., et al. 2011, Sol. Phys., 268, 1
Betancort-Rijo, J. 1990, MNRAS, 246, 608
Betancort-Rijo, J. 1991, Phys. Rev. A, 43, 2694
Cattaneo, F. 1999, ApJ, 515, L39
Centeno, R., Socas-Navarro, H., Lites, B., et al. 2007, ApJ, 666, L137
Chapman, D. G. 1951, University of California Publications in Statistics, 1, 131
Chertkov, M., Falkovich, G., Kolokolov, I., & Vergassola, M. 1999, Phys. Rev. Lett., 83, 4065
Cochran, W. G. 1978, in Contributions to Survey Sampling and Applied Statistics, ed. H. A. David (New York: Academic), 3
Colberg, J. M., Pearce, F., Foster, C., et al. 2008, MNRAS, 387, 933
Cranmer, S. R. 2009, Living Rev. Sol. Phys., 6, 3
Cranmer, S. R., & van Ballegooijen, A. A. 2010, ApJ, 720, 824
Danilovic, S., Beeck, B., Pietarila, A., et al. 2010, ApJ, 723, L149
Gaite, J. 2005, Eur. Phys. J. B, 47, 93
Gaite, J. 2009, J. Cosmol. Astropart. Phys., JCAP11(2009)004
Gömöry, P., Beck, C., Balthasar, H., et al. 2010, A&A, 511, A14
Ishikawa, R., & Tsuneta, S. 2009, in ASP Conf. Ser. 415, The Second Hinode Science Meeting: Beyond Discovery-Toward Understanding, ed. B. Lites, M. Cheung, T. Magara, J. Mariska, & K. Reeves (San Francisco, CA: ASP), 132

Ishikawa, R., & Tsuneta, S. 2010, ApJ, 718, L171
Ishikawa, R., Tsuneta, S., Ichimoto, K., et al. 2008, A&A, 481, L25
Kauffmann, G., & Fairall, A. P. 1991, MNRAS, 248, 313
Krebs, C. J. 2008, Ecology: The Experimental Analysis of Distribution and Abundance (6th ed.; San Francisco, CA: Pearson Benjamin Cummings)
Manso Sainz, R., Landi Degl' Innocenti, E., & Trujillo Bueno, J. 2004, ApJ, 614, 89
Manso Sainz, R., Martínez González, M. J., & Asensio Ramos, A. 2010, A&A, 531, 9
Martínez González, M. J., & Bellot Rubio, L. R. 2009, ApJ, 700, 1391
Martínez González, M. J., Collados, M., Ruiz Cobo, B., & Solanki, S. K. 2007, A&A, 469, L39
Martínez González, M. J., Manso Sainz, R., Asensio Ramos, A., & Bellot Rubio, L. R. 2010b, ApJ, 714, L94
Martínez González, M. J., Manso Sainz, R., Asensio Ramos, A., & Belluzzi, L. 2012, MNRAS, 419, 153
Martínez González, M. J., Manso Sainz, R., Asensio Ramos, A., López Ariste, A., & Bianda, M. 2010a, ApJ, 711, L57
Martínez Pillet, V., Del Toro Iniesta, J. C., Álvarez-Herrero, A., et al. 2011, Sol. Phys., 268, 57
Moreno-Insertis, F. 2012, in ASP Conf. Ser. 455, 4th Hinode Science Meeting: Unsolved Problems and Recent Insights, ed. L. Rubio, F. Reale, & M. Carlsson (San Francisco, CA: ASP), 91
Parnell, C. E., DeForest, C. E., Hagenaar, H. J., et al. 2009, ApJ, 698, 75
Pietarila, A., Cameron, R. H., Danilovic, S., & Solanki, S. K. 2011, ApJ, 729, 136
Politzer, H. D., & Preskill, J. P. 1986, Phys. Rev. Lett., 56, 99
Ravelet, F., Berhanu, M., Monchaux, R., et al. 2008, Phys. Rev. Lett., 101, 074502
Schrijver, C. J., & Title, A. M. 2003, ApJ, 597, L165
Seber, G. A. F. 2002, The Estimation of Animal Abundance and Related Parameters (Caldwell, NJ: Blackburn Press)
Solanki, S. K. 1993, Space Sci. Rev., 63, 1
Solanki, S. K., Barthol, P., Danilovic, S., et al. 2010, ApJ, 723, L127
Stenflo, J. O. 1982, Sol. Phys., 80, 209
Tikhonov, A. V., & Karachentsev, I. D. 2006, ApJ, 653, 969
Tobias, S. M., & Cattaneo, F. 2008, Phys. Rev. Lett., 101, 125003
Trujillo Bueno, J., Shchukina, N., & Asensio Ramos, A. 2004, Nature, 430, 326